Journal of Hazardous Materials 184 (2010) 273–280

Contents lists available at ScienceDirect

Journal of Hazardous Materials

journal homepage: www.elsevier.com/locate/jhazmat

Photocatalytic degradation of methylene blue by TiO_2–Cu thin films: Theoretical and experimental study

Hudson W.P. Carvalho[a,*], Ana P.L. Batista[b], Peter Hammer[a], Teodorico C. Ramalho[c]

[a] Unesp – Univ. Estadual Paulista, Institute of Chemistry, 14801-970 Araraquara-SP, Brazil
[b] University of São Paulo, Institute of Chemistry, 05508-000 São Paulo-SP, Brazil
[c] University Federal of Lavras, Chemistry Department, 37200-000 Lavras-MG, Brazil

ARTICLE INFO

Article history:
Received 1 June 2010
Received in revised form 22 July 2010
Accepted 8 August 2010
Available online 14 August 2010

Keywords:
Photocatalysis
TiO_2
Methylene blue
Cu
XPS

ABSTRACT

In this work the effect of doping concentration and depth profile of Cu atoms on the photocatalytic and surface properties of TiO_2 films were studied. TiO_2 films of about 200 nm thickness were deposited on glass substrates on which a thin Cu layer (5 nm) was deposited. The films were annealed during 1 s to 100 °C and 400 °C, followed by chemical etching of the Cu film. The grazing incidence X-ray fluorescence measurements showed a thermal induced migration of Cu atoms to depths between 7 and 31 nm. The X-ray photoelectron spectroscopy analysis detected the presence of TiO_2, Cu_2O and Cu^0 phases and an increasing Cu content with the annealing temperature. The change of the surface properties was monitored by the increasing red-shift and absorption of the ultraviolet–visible spectra. Contact angle measurements revealed the formation of a highly hydrophilic surface for the film having a medium Cu concentration. For this sample photocatalytic assays, performed by methylene blue discoloration, show the highest activity. The proposed mechanism of the catalytic effect, taking place on Ti/Cu sites, is supported by results obtained by theoretical calculations.

1. Introduction

There are several treatment techniques for wastewaters remediation, among them, advanced oxidative processes based on hydroxyls radicals (•OH) are of particular importance [1]. One way to produce •OH radicals consists in the irradiation of wide band gap semiconductors by UV light. The generated valence band holes and conduction electrons react with the surface hydroxyl groups and oxygen molecules adsorbed on the surface of the catalyst, forming hydroxyl radicals and super oxide radical ions, respectively. The high activity of these species is used to oxidize organic compounds. Moreover, the direct reaction between holes and organic pollutant also produces radicals, depending on the electronic properties of the target substance and the photocatalyst. In this case, the radical derived from pollutant molecule can react with both •OH radicals and dissolved oxygen [2].

TiO_2 is largely utilized as photocatalyst and various studies have been employed to enhance its photocatalytic activity using metal dopants. The metal doping process can be homogenous, using the sol–gel method (more common), or restricted to the surface by metal deposition. Arabatzis et al. have doped TiO_2 thin films with different loads of Au (0.40, 1.11, 2.01 and 3.61 at.%) by electron beam deposition. The thin films were employed to decompose an azo-dye colorant, showing the highest activity for 1.11 at.% load of Au [3]. The surface of TiO_2 nanoparticles modifieid by Zn oxide, and zinc aetate was used to evaluate its photocatalytical activity for methyl orange degradation, showing in both cases a higher activity than pure TiO_2 [4]. Dahyl et al. have doped TiO_2 nanoparticles sol by Ni acetylacetonate using high loads of Ni. The sample doped with 10% mol of Ni has shown the best performance to decompose a eiosine solution. The authors explained the increase on TiO_2 activity as due the increase of the Ti^{3+}/Ti^{4+} ratio [5].

In this context, one potential metal dopant for TiO_2 surfaces is copper, a metal of relative abundance and low cost. This work is aimed to investigate the influence of the Cu depth profile on the structural and catalytic properties of the TiO_2 surface. For this purpose, grazing incidence X-ray fluorescence (GIXRF), X-ray photoelectron spectroscopy (XPS) and UV–vis spectroscopy were employed to analyze the Cu depth profile and the surface structure. The wettability of the doped surface was investigated by contact angle measurements and the photocatalytic activity was studied by monitoring the decomposition process of methylene blue, used as model substance. Furthermore, the catalytic process was modeled by theoretical calculations based on a titanium oxide cluster.

* Corresponding author. Tel.: +55 16 3301 6886.
E-mail address: hudsonwpc@yahoo.com.br (H.W.P. Carvalho).

0304-3894/$ – see front matter © 2010 Elsevier B.V. All rights reserved.
doi:10.1016/j.jhazmat.2010.08.033

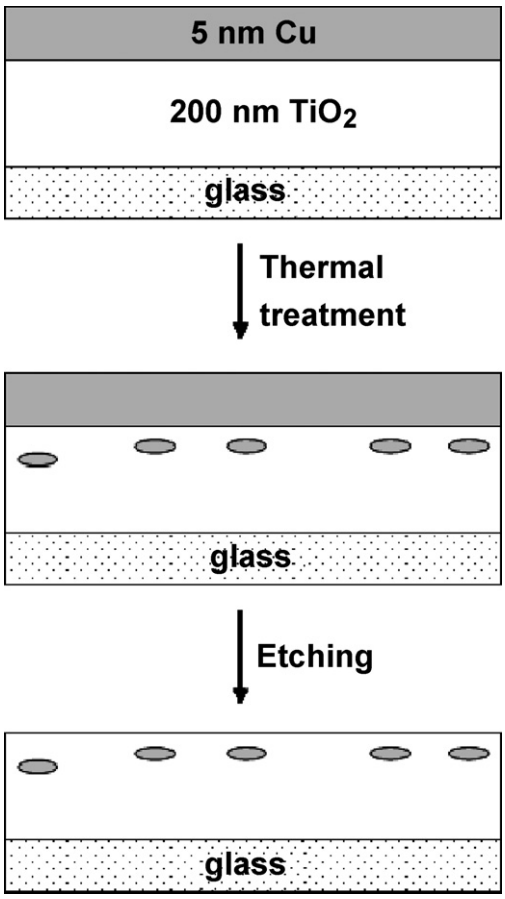

Fig. 1. Schematic sequence of sample preparation.

2. Experimental

2.1. Sample preparation

In the first step of the sample preparation process, shown in Fig. 1, 200 nm thick TiO_2 films were deposited on glass substrates (2 cm × 2 cm, borosilicate, Corning 7070) by DC sputtering (Balzers BA510). The main chamber base pressure was kept at 2×10^{-7} mbar, Ti (99.999%) was employed as target and the reactive gas mixture consisted of O_2 (99.99%) and Ar (99.99%). On the top of the TiO_2 film a 5 nm thick copper layer was deposited by DC sputtering using a Cu target (99.999%) and Ar (99.99%) working gas. In both depositions the adjusted power was 800 W.

The photocatalyst materials were obtained by thermally induced diffusion of Cu atoms into the TiO_2 films. For this purpose, the samples were submitted to thermal treatment for 1 s at 100 °C and 400 °C in argon atmosphere, using a rapid thermal processing system (RTA AG Heat Pulse 410). A set of non-annealed samples was used as a reference. After annealing, the Cu films were removed by chemical etching (10 mL hydrogen peroxide (30%, v/v), 50 mL of sulphuric acid and 440 mL of water; corrosion rate of 1 μm min^{-1}), leaving only a Cu doped TiO_2 surface region [6].

2.2. Characterization

The surface morphology was investigated by Atomic Force Microscopy (AFM). The images were collected under ambient conditions using an Agilent 5500 microscope operating in acoustic AC mode. Silicon tips (NanoWorld) with spring constants of 42 N m^{-1} and 320 kHz resonance frequency were used.

The X-ray diffraction (XRD) patterns were measured at room temperature using a Siemens D5000 X-ray diffractometer. The Cu-*K*α radiation with λ = 0.154 nm was used as the X-ray source.

Contact angle measurements were carried out by the sessile drop method using an OCA-20 Contact Angle System (DataPhysics Instruments). The Cu doped TiO_2 surface treated at room temperature, 100 °C and 400 °C, referred as TiO_2–Cu-RT, TiO_2–Cu-100 and TiO_2–Cu-400, were tested using liquids with different polarity and surface tension: glycerol ($\gamma_{L,V}$ = 65 mN/m), NaCl 3.5% solution ($\gamma_{L,V}$ = 73 mN/m) and ultra pure water ($\gamma_{L,V}$ = 72 mN/m) (MlliQ Millipore). A drop of the liquid (10 μL) was placed, with 1 μL/s velocity, on the film surface, and the contact angle was measured on three different positions for each film. To guarantee a clean surface the samples were cleaned in ultrasonic bath containing isopropylic alcohol and than dried in a jet of dry nitrogen. The accuracy of the contact angles was estimated as ±1% [7].

The absorption UV–vis spectra were recorded using a Cary 500 spectrophotometer. The optical gaps were determined from the intersection of the energy axis and the extrapolated line from the linear portion of the absorption threshold.

The grazing incidence X-ray fluorescence (GIXRF) measurements were performed at the XRF beamline of the Brazilian Synchrotron Light Laboratory (LNLS). The synchrotron radiation, produced by the DO9B (15°) bending magnet of the storage ring, was monochromatized by double crystal "channel-cut" monochromator equipped with a Si (1 1 1) crystal. The beam intensity was monitored using an ionization chamber. The X-ray fluorescence and scattered radiation coming from the sample was detected by an Ultra-LEGe solid state detector. Samples were placed in a special holder attached to a high resolution goniometer (0.001° angular resolution). The monochromatic beam was collimated with orthogonal slits to 4 mm × 0.2 mm in the horizontal and vertical direction, respectively. The selected beam energy was 9.5 keV, a value slightly above the K absorption edge for Cu. The angular dependence of the fluorescence signal was measured below and above the critical angle for total external reflection of the incident X-rays, covering an angular range between 0° and 1°.

X-ray photoelectron spectroscopy (XPS) was employed to determine the composition of the surface layer and the chemical environment of Ti and Cu using a commercial spectrometer (UNI-SPECS-UHV). The Mg-Kα line was used (hν = 1253.6 eV) and the analyzer pass energy was set to 10 eV. The inelastic background of the C 1s, O 1s, Ti 2p, and Cu 2p electron core-level spectra and the Auger Cu LMM peak was subtracted using Shirley's method. The binding energies of the spectra were corrected using the hydrocarbon component of adventitious carbon fixed at 285.0 eV. The composition of the surface region was determined from the ratio of the relative peak areas corrected by Scofield sensitivity factors of the corresponding elements. The spectra were fitted without placing constraints using multiple Voigt profiles. The width at half maximum (FWHM) of the XPS components varied between 1.5 and 2.0 eV and the accuracy of the peak positions was ±0.1 eV. The precision of the atomic concentrations of the detected elements was estimated as ±5%.

2.3. Photoactivity measurements

The measurements were carried out with 50 μL of hydrogen peroxide (30%, v/v) (Merck) and 5 mL (30 mg L^{-1}) methylene blue (Petroquímios) at pH 6.5. The degradation of the methylene blue solution was irradiated using a high-pressure mercury lamp (Philips 20 W) at 25 °C. Samples were taken at intervals of 10, 45 and 120 min, and the dye photodegradation was monitored by measuring the absorbance at 665 nm using a 1600 UV-vis spectrophotometer (Shimadzu UVPC).

Table 1
Contact angle and surface free energy determined for different solvents.

Thin film	Contact angle θ (°)[a]			Surface energy (mN/m)	Dispersion component (mN/m)	Polar component (mN/m)
	H_2O	NaCl	3.5% Glycerol			
TiO_2–Cu-RT	35	27	42	62	2	60
TiO_2–Cu-100	8	9	30	95	>1	95
TiO_2–Cu-400	51	46	41	50	19	31

[a] Estimated experimental error: ±1%.

2.4. ESI-MS study

To identify the intermediates formed during the methylene blue decomposition, mass spectroscopy coupled with electron spray ionization (ESI) was used (positive mode of an Agilent MS-ion trap mass spectrometer). After 20 min reaction a sample was collected and injected into the ESI source with a syringe pump at a flow rate of 5 mL min^{-1}, and the spectra were obtained as an average of 50 scans. The ESI conditions were as follows: heated capillary temperature of 325 °C, sheath gas (N_2) at a flow rate of 6 L min^{-1}, spray voltage of 4 kV and capillary voltage of 25 V.

2.5. Theoretical calculations

All calculations were carried out using the Gaussian 98 program package [8]. The hybrid B3LYP density functional method used includes Becke's 3-parameter nonlocal-exchange functional with the correlation functional [9]. For Ti and Cu atoms the aug-cc-pVQZ basis set was used, taking into consideration the effect of the diffuse function. For O and H atoms the cc-pVDZ basis sets was applied. The TiO_2 surface structure, represented by a $Ti_2O_9H_{10}$ cluster [10], was fully optimized without placing any constraints. Furthermore, after each optimization the nature of each stationary point was established by calculating and diagonalizing the Hessian matrix (force constant matrix). The unique imaginary frequency associated with the transition vector (TV), *i.e.*, the eigenvector associated with the unique negative Eigen value of the force constant matrix, has been characterized. Potential Energy Surface (PES) was evaluated using single-point energy calculation along the distance between two sites on the TiO_2 surface and metal. Moreover, the interaction of hydrogen peroxide with the cluster containing adsorbed Cu was studied for a variable distance of the peroxide molecule.

3. Results and discussion

Fig. 2 shows the AFM phase images of the TiO_2–Cu photocatalysts. Phase imaging is useful to distinguish material phases by sensing local variations in hardness, viscoeleasticity or adhesion [11]. The images show clear changes of the surface morphology as a function of thermal treatment. Although the XRD patterns (not shown) confirmed the amorphous nature of the films, the spots observed in the AFM phase images support the hypothesis of partial surface crystallization of the TiO_2 films. These spots, which increase in size with the annealing temperature, cannot be attributed to Cu particles, due to the low surface concentration of Cu, determined by the XPS analysis.

Since the photocatalytic reactions occur at the interface between solution and photocatalyst surface its wettability, related to the interplay of cohesive and adhesive liquid–solid interactions, is of particular interest. Contact angle measurements allow to determine the surface tension or energy, which is the key property influencing the wettability. Besides the chemical nature of the surface, wettability depends on the surface morphology and the type of the contact liquid [12]. The surface energy was determined via Young's equation: $\gamma_{sv} = \gamma_{sl} + \gamma_{lv}\cos\theta$, where θ is the measured contact angle and γ is the surface energy of the solid–vapour (sv), solid–liquid (sl) and liquid–vapour (lv) interface. The solid surface energy was extracted employing the Owens–Wendt–Rabel–Kaelble method [13,14]. A possible influence of the surface roughness on the wettability of the surfaces was investigated using AFM results. They have shown that the values of the RMS roughness of the samples were quite similar, varying form 0.6 nm for the RT sample to 0.8 nm for the sample annealed at 400 °C.

Table 1 displays the contact angle and the calculated surface energies of the samples. It can be observed that the TiO_2–Cu-100 film presents the highest surface energy and consequently quite small contact angles for all liquids employed. A similar behavior was reported for TiO_2–Mn films, where the contact angle for low dopant concentration decreases and then increases again for higher doping levels [15]. It is expected that the metal dopant reduces the Ti^{4+} to Ti^{3+} ratio on the surface. Then, the interaction of Ti^{3+} with water molecules leads to the formation of OH groups, which increase the wettability of the surface.

To determine the depth of the Cu ions below the TiO_2 surface, measurements of GIXRF were performed near the critical angle of total reflection, the experimental GIXRF data were than compared to the calculated X-ray fluorescence intensity curve [16]. The critical angle θ_c (in degrees) depends on the energy of the incident photons (E in keV), atomic number (Z), atomic mean mass (A) and on the density (ρ in g cm^{-3}). One approximation for the critical angle can be obtained by:

$$\theta_c \approx 1.65/E\sqrt{\frac{z}{A}\ \rho} \tag{1}$$

One fraction of the incident X-ray beam penetrates the TiO_2 surface. The penetration depth (Z_n) is a function of the energy or wavelength of incident photons (λ) and of the complex refractive index $n = 1 - \delta - i\beta$. The depth of penetration can be written as:

$$\begin{aligned} &\text{If} \quad \theta \ll \theta_c \quad Z_n \approx \lambda/4\pi\sqrt{2\delta} \\ &\text{If} \quad \theta \ll \theta_c \quad Z_n \approx \lambda/4\pi\sqrt{\beta} \\ &\text{If} \quad \theta \ll \theta_c \quad Z_n \approx \lambda\theta/4\pi\sqrt{\beta} \end{aligned} \tag{2}$$

The fluorescence intensity can be obtained as a function of incident angle. Employing a model were the Cu atoms are consider a buried layer of constant concentration below the TiO_2 surface, the theoretical fluorescence intensity was determined and fitted to the experimental data, thus allowing to determine the penetration depth of Cu dopant. In this model the fluorescence intensity can be written as:

$$I(\theta) = \frac{I_o c_a C[1 - R(\theta)]\theta}{Z_n} \tag{3}$$

where $I(\theta)$ is the fluoresce intensity as a function of the incident angle θ, the I_o is the intensity of incident photons, c_a is called area density (atoms cm^{-2}) and C is the scaling factor $[(12.4/4\pi E_o)/\beta]$. More details about the theoretical calculation of fluorescence intensity can be found in other studies [17].

Fig. 3 shows the experimental and the fitted theoretical curves for the diffusion depth of the Cu atoms. The results show that for

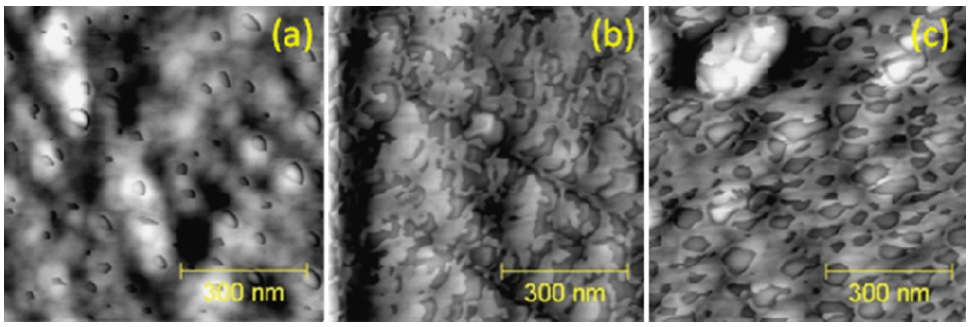

Fig. 2. Atomic force microscopy phase images of TiO_2–Cu films: (a) TiO_2–Cu-RT, (b) TiO_2–Cu-100, (c) TiO_2–Cu-400.

the TiO_2–Cu-RT sample (Fig. 3a) Cu reaches a depth of up to 9 nm. Zhou and Chen studied the diffusion of Cu in the TiO_2 as a function of time at room temperature by GIXRF and reported a depth of 5 Å after 30 min [18]. The GIXRF measured in this work were performed 20 days after Cu film deposition what might explain the higher diffusion depth. For the TiO_2–Cu-100 sample Cu was found about 11 nm deep (Fig. 3b) and in the TiO_2–Cu-400 film (Fig. 3c) a depth of Cu of about 30 nm was detected. These values are consistent with the diffusion-induced increase of the penetration depth with the temperature of the thermal treatment.

The UV–vis absorption spectra, displayed in Fig. 4, show a slight red-shift to the visible region and a small increase of the absorption with increasing thermal treatment. Considering that the Cu dopant is located in a depth range between few nanometers and 30 nm and that the band gaps of Cu_2O and CuO of 1.7 and 2.1 eV, respectively, are smaller than that of TiO_2 (3.2 eV), it can be concluded that the temperature induced doping process was efficient in decreasing the band gap and increasing the absorption of the samples. Consequently, the band gap values decreased from 3.2 eV for theTiO_2–Cu-RT to 3.15 eV for TiO_2–Cu-100 and 3.1 eV for the TiO_2–Cu-400 sample.

Although several studies so far have reported on the catalytic activity of Cu doped TiO_2, none of them has explored the particular catalytic proprieties of the system as a function of the Cu profile. The results presented below evidenced that the surface activity can be modified by different concentration profiles of Cu in the surface region of the TiO_2 film. To investigate this aspect in more details, XPS measurements were performed to analyze the surface region of the samples before and after reaction with methylene blue and H_2O_2.

The XPS data of the elemental composition of the surface, obtained without sputter cleaning, are shown in Table 2. As expected, the Ti to O ratio remains constant and the Cu concentration increases with the temperature of the thermal treatment, showing the highest Cu content of about 2.5 at.% for the TiO_2–Cu-400 sample. This data confirmed that the observed small red-shift of the UV–vis spectra absorbance is related to the higher Cu content of the surface region of the TiO_2 film. After photocatalytic tests the Cu concentration decreased probably due to the contamination of the surface by additional carbon species, which increased from about 35 at.% to 45 at.% after photocatalytic tests, as well as sulphur and nitrogen impurities, related to the fragments of methylene blue (Table 2). For the not tested samples additional XPS measurements were carried out at a take-off angle of 30°, corresponding to the half of the typical sampling depth of about 3 nm, to probe the slope of the depth profile in the diffusion layers. The results show a relatively flat copper concentration profile few nanometers below the surface, indicating a homogeneous doping of the active surface region of the film.

The structural analysis performed by XPS (Fig. 5) indicates for all films the presence of only one structural component of Ti $2p_{3/2}$ peak at 458.6 eV, attributed to the TiO_2 phase. A representative Cu $2p_{3/2}$ spectrum obtained for the TiO_2–Cu-100 sample, shown in Fig. 4, displays only one fitted component at 932.2 eV indicating the possible presence of both the Cu_2O and the metallic Cu phase. Due to the difficulty to separate the contributions of these phases in the photoemission spectrum, the Auger $L_3M_{45}M_{45}$ peak was recorded to determine the Cu^0 to Cu_2O ratio. The analysis of the differentiated Auger spectrum showed the predominance of the Cu_2O phase located at a kinetic energy of 916.5 eV (Insert of Fig. 5). A smaller signal at about 918.7 eV is related to the metallic phase. These values are close to those found for Cu_2O and Cu bulk material of 316.6 eV and 918.6 eV, respectively [19]. No significant influence of the TiO_2 matrix on the peak Cu energies was observed, however it cannot be excluded that a small fraction of Cu species was introduced into the TiO_2 lattice as substitutional dopant, induced by the thermally enhanced diffusion process. Furthermore, the Cu^0 to Cu_2O ratio of about 0.25 remained almost constant with increasing thermal treatment. It is interesting to note that one significant difference observed between the TiO_2–Cu-100 film and the other samples was its strong O 1s component at 532.1 eV, indicating for this film a larger number of hydroxile surface groups (not shown).

The photocatalytic activity of the films was evaluated by monitoring the methylene blue degradation. Fig. 6 displays the absorbance of methylene blue under UVA irradiation as a function of time. It can be observed that in absence of the catalyst methylene blue is subjected to photolysis resulting in a small decrease of the absorbance after 2 h irradiation. Addition of H_2O_2 to the medium

Table 2
Quantitative X-ray photoelectron spectroscopy analysis of TiO_2–Cu photocatalysts before and after reaction with methylene blue, performed at a take-off angle of 90° and 30°.*

Photocatalyst	Ti		O		Cu (at.%)[a]		S	N
TiO_2–Cu-RT before	29.0	28.8*	70.5	70.6*	0.5	0.6		
TiO_2–Cu-100 before	29.4	29.2*	69.9	70.2*	0.7	0.6		
TiO_2–Cu-400 before	28.6	28.4*	68.9	69.3*	2.5	2.3		
TiO_2–Cu-RT after	30.0		66.5		<0.1		1.1	2.3
TiO_2–Cu-100 after	29.6		67.5		0.1		1.0	1.8
TiO_2–Cu-400 after	28.4		68.3		1.0		0.7	1.6

* Estimated experimental error: ±5%.

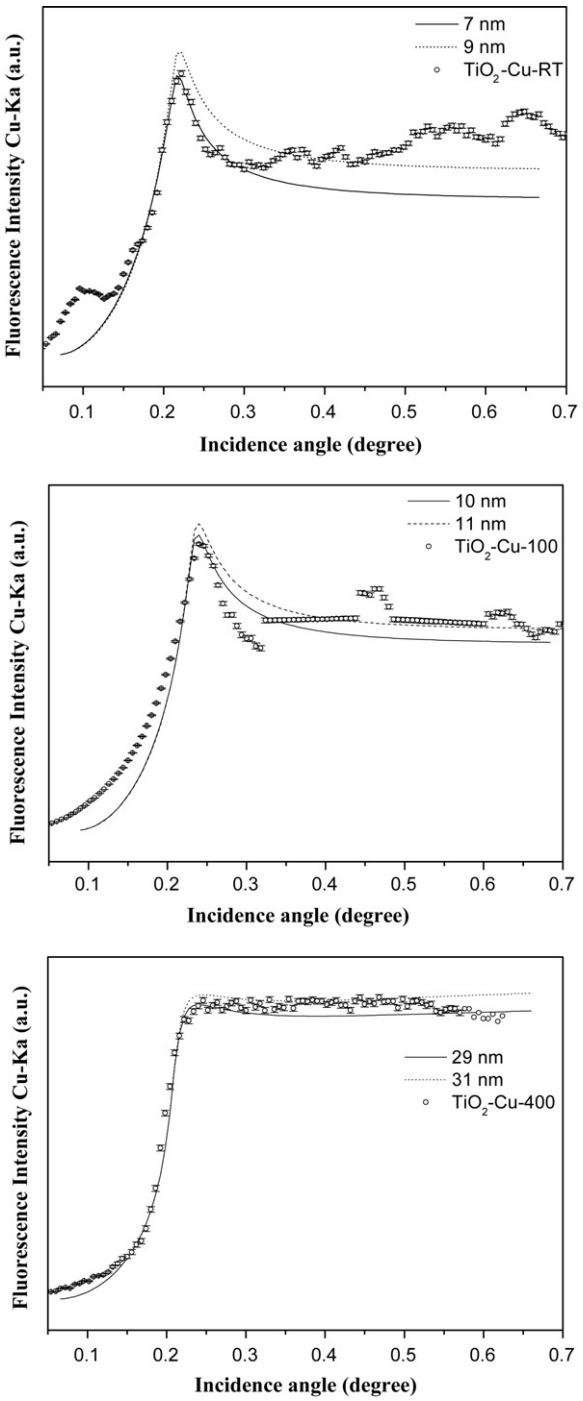

Fig. 3. Experimental and fitted grazing incidence X-ray fluorescence curves for samples of Fig. 2.

led to an accelerated methylene blue decomposition due to the formation of highly oxidant •OH. Compared to the methylene blue solution containing only H_2O_2 or pure TiO_2/H_2O_2, the incorporation of the Cu into catalyst improved significantly the degradation of the colorant, demonstrating its superior photocatalytic activity. Furthermore, the comparison of the three catalysts shows that the TiO_2–Cu-100 film possesses the highest photoactivity. This finding is in agreement with the contact angle data, indicating that this surface is more hydrophilic, thus enhancing the interaction between medium and catalyst. But this is just one aspect, there is another effect that could be related with oxygen vacancies produced by Ti^{3+} formation. Ti^{4+}, Cu^{+} or Cu^{2+} can act as trapping sites of photoinduced electron, increasing the electron–hole pair life-time, and thus enhancing the probability of reactions between electron-hole pairs and the H_2O, H_2O_2 and OH^- species.

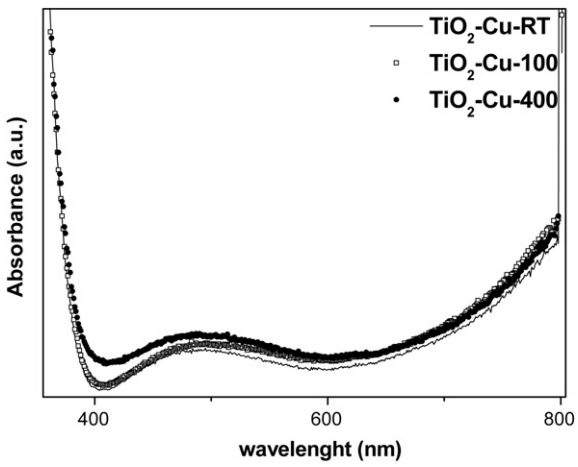

Fig. 4. Ultraviolet–visible spectra for samples of Fig. 2.

The observation of a higher catalytic activity for the sample with intermediary Cu concentration is supported by results obtained by Xin et al. [20]. The authors argue that this occurs due the role of Cu in modulating the Ti^{4+}/Ti^{3+} ratio and oxygen vacancies. At high Cu concentration the amount of oxygen vacancies increases, which act as recombination centers of generated electron–hole pairs.

It is suggested that there are at least two active regions on the catalysts surface, the TiO_2 and Cu sites. In the first case, the trans-

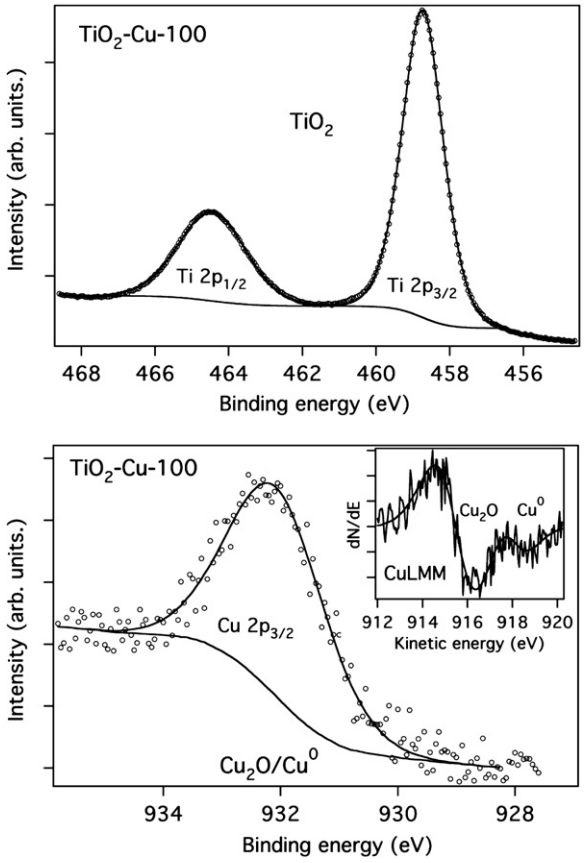

Fig. 5. X-ray photoelectron spectroscopy Ti 2p and Cu 2p core-level spectra and the Cu $L_3M_{45}M_{45}$ Auger peak of sample TiO_2–Cu-100.

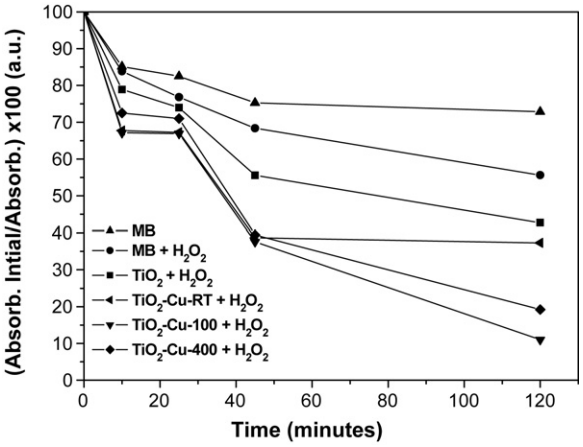

Fig. 6. Photocatalytic discoloration of methylene blue (MB) by TiO_2–Cu thin films.

fer of electrons and holes in a reaction with H_2O_2, H_2O, O_2 and methylene blue can take place on the TiO_2 surface leading to oxidized or reduced species. These mechanisms are well explored in several photocatalytic studies [21]. In the case o copper doping, the reaction between Cu^0 or Cu^+ with the H_2O_2 results in a Fenton-like mechanism, according to the following reactions:

$$\begin{aligned} &Cu^0 \text{ or } Cu^+ + H_2O_2 \rightarrow Cu^+ \text{ or } Cu^{2+} + OH^- + \cdot OH \\ &TiO_2 + h\nu \rightarrow h^+/e^- \\ &Cu^+ \text{ or } Cu^{2+} + e^- \rightarrow Cu^0 \text{ or } Cu^+ \end{aligned} \quad (4)$$

It is well known that the pH value of the solution causes modifications of the TiO_2 surface. Here the reaction of H_2O_2 with Cu species led to an alkaline medium, due the generation of OH^-. In this condition the TiO_2 surface is negatively charged and a reaction of OH^- with holes leads to the formation of •OH, while the electrons can reduce Cu oxidized species or react with H_2O_2 forming •OH [22]. This consideration is in agreement with the mass spectroscopy results, shown below, which indicate that methylene blue is decomposed by •OH.

This mechanism is consistent with a recent study, suggesting an enhanced catalytic decomposition of H_2O_2 on the Cu doped semiconductor surface [23]. The formation of •OH radical and the subsequent oxidation reaction of organic compounds were evidenced from the analysis of the ESI-MS spectra, shown in Fig. 7. The methylene blue cation signal can be identified at m/z = 284, 300 and at 316, related to successive hydroxylation of the molecule due to •OH attack. The other signals correspond to the fragmentation of the molecular structure. This result is in agreement with several studies reporting the complete mineralization of the colorant by hydroxyl radicals [24].

The effect of peroxide action in the TiO_2–Cu system was confirmed by theoretical calculations. Using a $Ti_2O_9H_{10}$ cluster model, firstly, the possible interaction sites of Cu on the TiO_2 surface were investigated in the presence and absence of peroxide. Here it is important to mention that nonbonded interactions play an important role in structural chemistry. Attractive, albeit noncovalent, nonbonded interactions modulate the conformations of virtually all molecular assemblies [25]. In the solid state, a close intramolecular contact may result from either an attractive interaction or as a consequence of external forces imposed by crystal packing. Despite of its great importance, the effect of doping depth profile on photocatalytic activity of TiO_2 based materials was not very much studied, and in particular, surprisingly little detailed computational work was reported on this subject.

In order to investigate the interaction between the dopant and the TiO_2 surface, two different sites, named A and B, were studied. The representation of these sites is shown in Fig. 8(a), and (b) displays the corresponding potential energy curves. In Fig. 8(a) it can be observed that the energetically preferred B site (solid circle around the Ti atom) contains a larger number of oxygen neighbors than the A site (dashed circle). This is related to an efficient transfer of valence electrons from the Cu atoms to TiO_2 at B sites. This charge transfer occurs only through interaction of the Cu atoms with oxygen and the subsequent formation of a strong bond [26]. This fact can be better understood considering that as more oxygen is being added to the surface , the interaction of Cu atoms with TiO_2 enhances the formation of additional •OH radicals. Furthermore, the potential curve of the B site in the presence of H_2O_2 shows a significant reduction of the energy of the system. These results reinforce the suggestion that there is a favorable interaction between H_2O_2 molecules and the TiO_2 surface, as observed in catalytic tests and contact angle measurements (Fig. 6 and Table 1).

In addition, density functional theory (DFT) data can also in principle rationalize the UV–vis results. It is important to mention that the precision of this calculation level is estimated about 3 kcal mol^{-1} [27]. The slight decrease of the band gap values, from 3.2 eV for TiO_2–Cu-RT to 3.1 eV for the TiO_2–Cu-400 sample, can be interpreted as due to the influence of the electronic and relativistic effects of the Cu-doping on the material surface. The relativistic effect of Cu is very weak and the energy gaps between orbital 3d and 4s of Cu are relatively high. Then, the orbital interaction between the molecular orbital of H_2O_2 and the orbital 4s of Cu are weaker. This is in contrast to interactions between the 4s orbital of Cu and the dangling bond on the Ti surface, which are considered stronger. Thus, the theoretical data reinforce the interpretation of GIXRF and catalytic activity data.

The identification of reaction intermediates was performed by ESI-MS measurements during the oxidation of the methylene blue

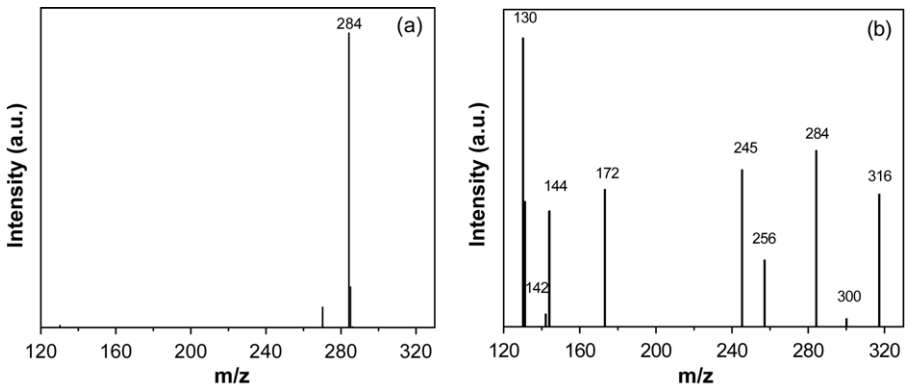

Fig. 7. Mass spectrometry spectra of (a) pure methylene blue colorant, and (b) after 10 min of started photocatalytic reaction.

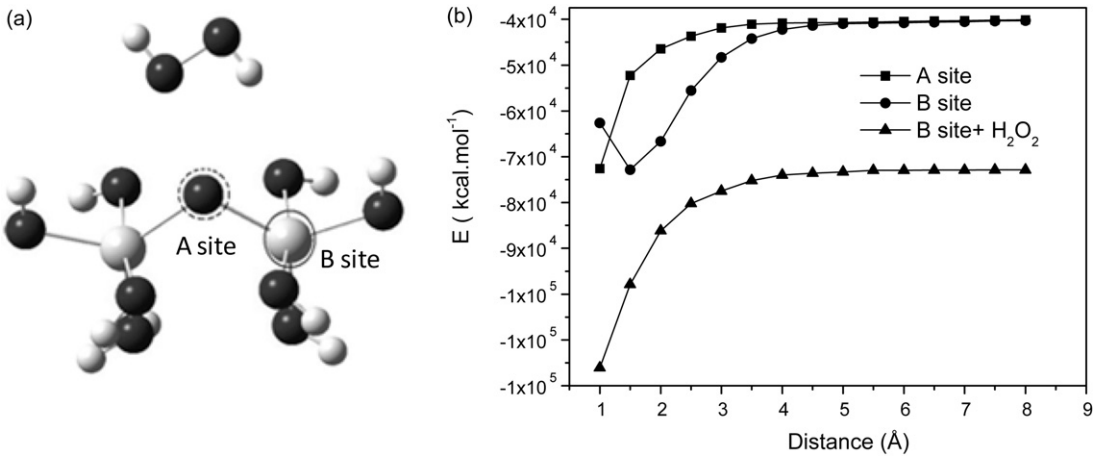

Fig. 8. (a) $Ti_2O_9H_{10}$ cluster with sites: "A", dash circle and "B", solid circle, together with representation of H_2O_2. (b) Potential energy curves obtained for the interaction between the TiO_2 cluster and the Cu dopant at sites A and B including the interaction of peroxide at site B.

Table 3
Gibbs free energy of II and III intermediates using B3LYP/6-31 + G(d,p).

Intermediate	Hydroxyl position	Δ (kcal mol^{-1})
II	2	0.00
	3	+3.30
	N	+7.86
	S	+8.68
	5	+6.65
III	2, 2′	0.00
	2, 5′	+34.69
	3, 2′	+11.73
	3, 3′	+14.26
	3, 5′	+3.25
	5, 5′	+21.22

dye (Fig. 7). In order to shed more light on the model of the overall reaction mechanism of the catalytic activity, calculations of the Gibbs free energy for the stability of the intermediates were performed. All discussions concerning the energy differences and the energy barriers refer to the enthalpy term corrected for the zero point energy at 298.15 K. The resulting energies values and corresponding structures are presented in Table 3 and Fig. 9. From these calculations a good agreement was found between the modeled and experimental geometry for the methylene blue molecule [28]. According to the data listed in Table 3, it can be observed that the hydroxyl group on C2 position of intermediate II is about +3.30 and +6.65 kcal mol^{-1} more stable than the alternative C3 and C5 position, respectively.

These results put in evidence that the preferential reaction site for •OH in this Fenton-like process is the position 2 (C2) of the methylene blue structure, resulting in a fragment corresponding to m/z = 300 (Fig. 7). Further calculations revealed that the hydroxylation occurs on C4 (see Table 3), which explains the resulting intense fragment corresponding to m/z = 316 (Fig. 7). From these theoretical results, compounds II and III (Fig. 9) are supposed to be more stable and can be therefore experimentally detected. Moreover, the reaction path may still involve other hydroxylations. From these results, the third hydroxylation would more likely occur at 5′ position. This is a crucial step, as it would simultaneously lead to the formation of hydroquinone or hydroquinone-like intermediates generated by the •OH attack.

A reaction mechanism was earlier proposed for the interaction between Fenton reagents and aromatic compounds [29] and Orange II dye [30], which involves the generation of hydroquinone or hydroquinone-like and the redox cycle of hydroquinone/quinone in the Fenton reaction. That is an unstable key-intermediate that indicates a high probability of a quick rupture of both chemical bonds C1–C2 and C5–C6 (Fig. 9). This could justify the formation of V (m/z = 130). Nevertheless, the presence of •OH in the reaction medium, the oxidation of V probably occurs, which consequently generates the stable specie VI, with m/z = 161.

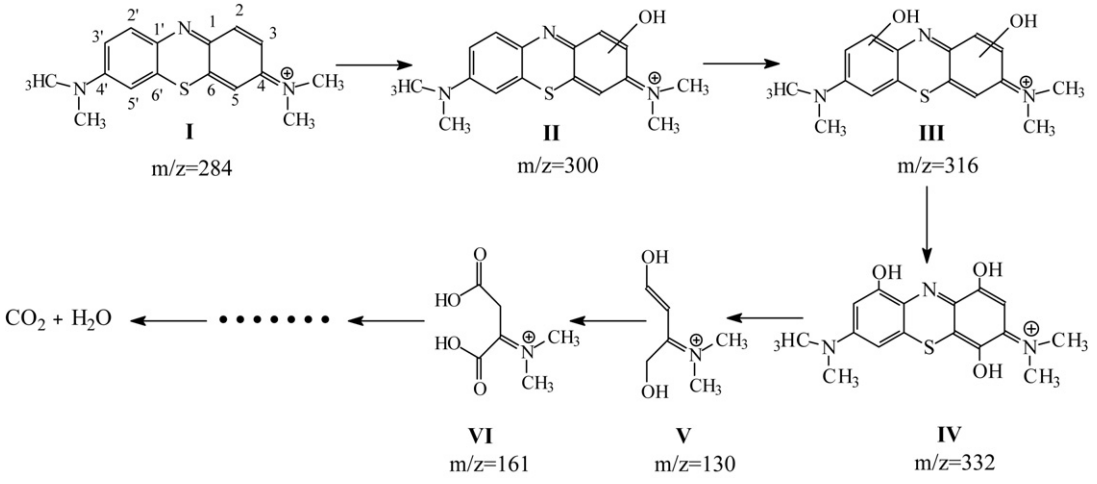

Fig. 9. Reaction scheme with the proposed route for methylene blue degradation.

These calculations are in good agreement with experimental data (Fig. 7).

Based on previous studies [24,27] and the results displayed in Fig. 7, we propose that the reaction initiated with the activation of H_2O_2 by the doped TiO_2 film followed by the transfer of $^{\bullet}OH$ radicals to the organic dye, producing different fragment compounds as showed by the intense MS signals. The experimental results suggest that the proposed catalytic mechanism is based on the activation of H_2O_2 *via* a Fenton-like mechanism at active Ti–O–Cu sites to form increased quantities of $^{\bullet}OH$ radicals.

4. Conclusion

Surface properties and photocatalytic activity of copper doped TiO_2 films were investigated for different surface concentration profiles of Cu. The GIXRF measurements indicate that the thermal treatment causes a migration of Cu atoms below the surface to depths which varies between 7 and 31 nm, causing a small red-shift and increasing absorption of the UV–vis spectra. The contact angle measurements have shown that films with a medium Cu-doping concentration of about 1 at.% own the most hydrophilic surface. Photocatalytical tests performed by methylene blue discoloration have confirmed for this film a higher photocatalytic activity. According to the results obtained by theoretical calculations the enhanced catalytic efficiency can be explained by a Fenton-like mechanism induced by the formation of active Ti–O–Cu sites. The XPS analysis confirmed the presence of Cu^+ and Cu^0 species on the TiO_2 surface and evidenced their homogeneous distribution in the active region of the film. Theoretical calculations performed at DFT level support several experimental results as band gap changes, affinity of H_2O_2 by TiO_2 doped with Cu. The ESI-MS spectra allied to theoretical calculations allowed to propose the fragmentation route of methylene blue.

Acknowledgments

The authors are grateful to The State of São Paulo Research Foundation (FAPESP), The National Council for Scientific and Technological Development (CNPq), Brazilian Synchrotron Light Source (LNLS), The State of Minas Gerais Research Foundation (FAPEMIG) and CAPQ-DQI-UFLA for financial support.

References

[1] M.A. Brown, S.C. Vito, Predicting azo dye toxicity, Crit. Rev. Environ. Sci. Technol. 23 (1993) 249.
[2] L. Zhang, J. Li, Z. Chen, Y. Tang, Y. Yu, Preparation of Fenton reagent with H_2O_2 generated by solar light-illuminated nano-Cu_2O/MWNTs composites, Appl. Catal. A 299 (2006) 292.
[3] I.M. Arabatzis, T. Stergiopoulos, D. Andreeva, S. Kitova, S.G. Neophytides, P. Falaras, Characterization and photocatalytic activity of Au/TiO_2 thin films for azo-dye degradation, J. Catal. 220 (2003) 127.
[4] J.C. Xu, Y.L. Shi, J.E. Huang, B. Wang, H.L. Li, Doping metal ions only onto the catalyst surface, J. Mol. Catal. A 219 (2004) 351.
[5] M. Dhayal, S.D. Sharma, C. Kant, K.K. Saini, S.C. Jain, Role of Ni doping in surface carbon removal and photo catalytic activity of nano-structured TiO_2 film, Surf. Sci. 602 (2008) 1149.
[6] H.W.P. Carvalho, A.P.L. Batista, R. Bertholdo, S.H. Pulcinelli, C.V. Santilli, Photocatalyst TiO_2–Co: the effect of doping depth profile on methylene blue degradation, J. Mater. Sci. (Published on line: 16 june 2010. doi:0.1007/s10853-010r-r4639-5).
[7] T. Watanabe, S. Fukayama, M. Myauachi, A. Fujishima, K. Hashimoto, Photocatalytic activity and photo-induced wettability conversion of TiO_2 thin film prepared by sol–gel process on a soda-lime glass, J. Sol–Gel Sci. Technol. 19 (2000) 71.
[8] A.E. Frisch, M.J. Frisch, G.W. Trucks, Gaussian03 User's Reference, Gaussian Inc., Wallingford, USA, 2003.
[9] A.D. Becke, Density-functional exchange-energy approximation with correct asymptotic behavior, Phys. Rev. 38 (1988) 3089.
[10] I. Onal, S. Soyer, S. Senkan, Adsorption of water and ammonia on TiO_2-anatase cluster models, Surf. Sci. 600 (2006) 2457.
[11] O.P. Behrend, L. Odoni, J.L. Loubet, N.A. Burnham, Phase imaging: deep or superficial? App. Phys. Lett. 7 (1999) 2551.
[12] D. Janssen, R. Palma, S. Verlaak, P. Heremans, W. Dehaen, Static solvent contact angle measurements, surface free energy and wettability determination of various self-assembled monolayers on silicon dioxide, Thin Solid Films 515 (2006) 1433.
[13] R.K. Bregg, Current Topics in Polymer Research, Nova Science Publisher, New York, 2005.
[14] J.O. Carneiro, V. Teixeira, A.J. Martins, M. Mendes, M. Ribeiro, A. Vieira, Surface properties of doped and undoped TiO_2 thin films deposited by magnetron sputtering, Vacuum 83 (2009) 1303.
[15] S.D. Sharma, K.K. Saini, C. Kant, C.P. Sharma, S.C. Jain, Photodegradation of dye pollutant under UV light by nano-catalyst doped titania thin films, Appl. Catal. B 84 (2008) 233.
[16] R. Klockenkämper, Total-Reflection X-ray Fluorescence Spectrometry, John Willey & Sons, New York, 1997.
[17] H.W.P. Carvalho, A.P.L. Batista, T.C. Ramalho, C.A. Pérez, A. Gobbi, The interaction between atoms of Au and Cu with clean Si (1 1 1) surface: a study combining synchrotron radiation grazing incidence X-ray fluorescence analysis and theoretical calculations, Spectrochim. Acta Part A 74 (2009) 292.
[18] J. Zhou, D.A. Chen, Controlling size distributions of copper islands grown on TiO_2(1 1 0)-(1 × 2), Surf. Sci. 527 (2003) 183.
[19] J.P. Espinós, J. Marales, A. Barranco, A. Caballero, J.P. Holgado, A.R. González-Elipe, Effect of surface species on Cu–TiO_2 photocatalytic activity, J. Phys. Chem. B 106 (2002) 6921.
[20] B. Xin, P. Wang, D. Ding, J. Liu, Z. Ren, H. Fu, Effect of surface species on Cu–TiO_2 photocatalytic activity, Appl. Surf. Sci. 254 (2008) 2569.
[21] D. Robert, B. Dongui, J.V. Weber, Heterogeneous photocatalytic degradation of 3-nitroacetophenone in TiO_2 aqueous suspension, Photochem. Photobiol. A 156 (2003) 195.
[22] W. Chu, W.K. Choy, T.Y. So, The effect of solution pH and peroxide in the TiO_2-induced photocatalysis of chlorinated aniline, J. Hazard. Mater. 141 (2007) 86.
[23] I.R. Guimarães, A. Giroto, L.C.A. Oliveira, M.C. Guerreiro, D.Q. Lima, J.D. Fabris, Synthesis and thermal treatment of Cu-doped goethite: oxidation of quinoline through heterogeneous Fenton process, Appl. Catal. B 91 (2009) 581.
[24] A. Esteves, L.C.A. Oliveira, T.C. Ramalho, M. Goncalves, A.S. Anastacio, H.W.P. Carvalho, New materials based on modified synthetic Nb_2O_5 as photocatalytic for oxidation of organic contaminants, Catal. Commun. 10 (2008) 330.
[25] T.C. Ramalho, T.L.C. Martins, L.E.P. Borges, J.D. Figueroa-Villar, Influence of non-bonded interactions in the kinetics of formation of chalcogenol esters from chalcogenoacetylenes, Int. J. Quantum Chem. 95 (2003) 267.
[26] L. Giordano, G. Pacchioni, T. Bredow, J.F. Sanz, Cu, Ag, and Au atoms adsorbed on TiO_2(1 1 0): cluster and periodic calculations, Surf. Sci. 471 (2001) 21.
[27] L.C.A. Oliveira, T.C. Ramalho, M. Gonçalvez, F. Cereda, K.T. Caravalho, M.S. Nazzaro, K. Spag, Pure niobia as catalyst for the oxidation of organic contaminants: mechanism study via ESI-MS and theoretical calculations, Chem. Phys. Lett. 446 (2007) 133.
[28] I. Ma, W. Song, C. Chen, W. Ma, J. Zhao, Y. Tang, Fenton degradation of organic compounds promoted by dyes under visible irradiation, Environ. Sci. Technol. 39 (2005) 5810.
[29] T.C. Ramalho, L.C.A. Oliveira, K.T.G. Carvalho, E.F. Souza, E.F.F. da Cunha, M. Nazzaro, The molecular basis for the behaviour of niobia species in oxidation reaction probed by theoretical calculations and experimental techniques, Mol. Phys. 107 (2009) 171.
[30] N.H. Ince, D.A. Hasan, B. Ustun, G. Tezcanli, Combinative dyebath treatment with activated carbon and UV/H_2O_2: a case study on Everzol Black-GSP, Water Sci. Technol. 46 (2002) 51.